MODELING THE PROPAGATION SAW TEST WITH DISCRETE ELEMENTS

Grégoire Bobillier[1,*], Johan Gaume[1,2], Alec van Herwijnen[1], Jürg Dual[3], Jürg Schweizer[1]

[1] *WSL Institute for Snow and Avalanche Research SLF, Davos, Switzerland*
[2] *EPFL Swiss Federal Institute of Technology, School of Architecture, Civil and Environmental Engineering, Lausanne, Switzerland*
[3] *Institute for Mechanical Systems, ETH Zurich, Zurich, Switzerland*

ABSTRACT: Dry-snow slab avalanche release is a multi-scale fracture process. It starts with the formation of a localized failure in a highly porous weak snow layer underlying a cohesive snow slab, followed by rapid crack propagation within the weak layer and finally a tensile fracture through the slab leading to its detachment. About 15 years ago, the propagation saw test (PST) was developed, a fracture mechanical field test that provides information on crack propagation propensity in weak snowpack layers. It has become a valuable research tool to investigate processes involved in crack propagation. While this has led to a better understanding of the onset of crack propagation, much less is known about the ensuing propagation dynamics. To analyze the dynamics of propagating cracks, we therefore modeled a three-dimensional PST with the discrete element method (DEM). Using cohesive ballistic deposition, we created a highly porous, anisotropic and brittle weak layer covered by a dense cohesive and isotropic snow slab. By tuning the contact law parameters between particles, we obtained realistic macroscopic behavior of snow deformation for the slab and the weak layer. We then simulated PSTs by cutting the weak layer with a numerical snow saw. The simulations reproduced the dynamics of crack propagation as observed in the field. Our results highlight the influence of the mechanical properties of the slab and weak layer on the stress distribution during crack propagation, the propagation distance before fracture arrest and the propagation speed.

KEYWORDS: Dry-snow slab avalanche, discrete element method, crack propagation.

1. INTRODUCTION

Dry-snow slab avalanches require the initiation and the propagation of a crack in a weak snow layer buried below cohesive slab layers. Rapid crack propagation occurs if the initial zone of damage is larger than a critical size or if the load exceeds a critical value. Weak layer fracture during crack propagation is generally accompanied by its structural collapse, as snow is a highly porous material. If crack propagation occurs across a steep slope a slab avalanche may release (McClung 1979, Schweizer, Jamieson et al. 2003).

Our knowledge of slab avalanche release at the slope scale is still limited, partly due to (i) the complex microstructure of snow, (ii) the highly porous character of weak layers, (iii) the spatial variability of snow layering, and (iv) the lack of adequate in-situ measurement methods for the relevant mechanical quantities. Nevertheless, our understanding of crack propagation has greatly improved by the introduction of the Propagation Saw Test (PST; van Herwijnen and Jamieson 2005, Gauthier and Jamieson 2006, Sigrist and Schweizer 2007). With the PST, many measurements can be performed at a scale that is less influenced by heterogeneity due to terrain. It allows analyzing crack propagation propensity and deriving mechanical quantities by e.g. particle tracking (van Herwijnen, Bair et al. 2016). However, no theoretical framework exists to interpret PST results in relation to snowpack properties and how those affect the dynamics of crack propagation. Numerical simulations can therefore be used to investigate fracture in snow in more detail.

The discrete element method (DEM) was recently used to model snow microstructure (Hagenmuller, Chambon et al. 2015) and crack propagation (Gaume, van Herwijnen et al. 2015). It allows generating highly porous samples and was used to perform 2D-simulations of the PST in agreement with field experiments. These recent studies opened a new avenue to study the processes of crack formation, propagation and collapse. Nevertheless, the oversimplified shape and the 2D character of the weak layer prevented a detailed analysis of the internal stresses during crack propagation.

Our objective is therefore to investigate the dynamics of crack propagation. We used a 3D discrete element model to reproduce the different types of snow layer structures and to have access to mechanical properties. To relate DEM param-

* Corresponding author address:
Grégoire Bobillier, WSL Institute for Snow and Avalanche Research SLF,
Fluelastrasse 11, CH-7260 Davos Dorf, Switzerland;
tel: +41 81 417 03 475
E-mail: gregoire.bobillier@slf.ch

eters to real-world values, we linked particle parameters to macroscopic snow behavior as observed in mechanical testing. Finally, we modeled a PST to highlight that these 3D simulations can be used to study the parameters that drive failure initiation and crack propagation dynamics.

2. METHODS

2.1 Discrete element model

The discrete element method (DEM) introduced by Cundall and Strack (1979) is a numerical tool commonly employed to study granular-like assemblies composed of a large number of discrete interacting particles. We used the PFC3D software developed by Itasca.

2.2 Formulation of the model

The particle contact law we used is called a parallel-bond model and was introduced by Potyondy and Cundall (2004). The parallel bond provides the mechanical behavior of a finite-sized piece of cement-like material deposited between the two contacting particles. The parallel-bond component acts in parallel with the classical linear contact model and establishes an elastic interaction between the particles. The mechanical parameters include the contact elastic modulus E_u, Poisson's ratio ν_u = 0.3, the restitution coefficient e_u = 0.1 and the friction coefficient μ_u = 0.2. If particles are bonded, the bond part will act in parallel to the contact part. The bonded part is described by the bond elastic modulus E_b, the bond Poisson's ratio ν_b = 0.3 and the bond strength. The bond failure behavior is characterized by its shear and tensile strength σ_s and σ_t. To reduce the number of variables we assume $E_u = E_b$ and $\sigma_s = \sigma_t$. For the parameters assumed to be constant, the same values were selected as described in Gaume, van Herwijnen et al. (2015) and Gaume, Löwe et al. (2017).

2.3 Slab generation and characterization

The slab layer is generated by cohesionless ballistic deposition, which allows creating a dense sample (Kadau and Herrmann 2011). Particle radius, which does not relate to a physical grain size in snow slabs, was fixed at r_b = 1.1 cm with 10% variability to avoid close packing. The porosity of the slab was equal to 35% and we adjusted particle density to obtain a slab density ρ_{slab} = 250 kg/m^3 corresponding to a typical mean slab density (van Herwijnen, Gaume et al. 2016). As will be shown below, this set up allows capturing the main macroscopic behavior consistent with laboratory experiments; it also reduces computational time.

We performed a large number of simulations to analyze the relation between macroscopic elastic behavior and particle elastic modulus E_u. Figure 1 shows the simulated macroscopic elastic modulus as function of E_u and a linear fit. In addition, by fixing the particle elastic modulus and varying particle strength over a large number of simulations, we also obtain a linear relation between the macroscopic strength and bond strength (not shown).

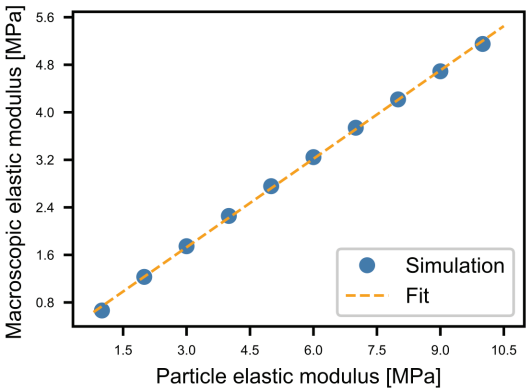

Figure 1: Slab macroscopic elastic modulus with elastic modulus of the slab particles obtained by simulating an unconfined load-controlled compression test.

2.4 Weak layer generation and characterization

Cohesive ballistic deposition (Löwe, Egli et al. 2007) was used to mimic the porous structure of weak layers consisting of faceted crystals as found in a natural snowpack. The natural formation process is more complex and includes temperature gradients and snow metamorphism. Nevertheless, we obtained a porosity of 80% and we adjusted the density of the particles to obtain a weak layer density ρ_{wl} = 120 kg/m^3. The weak layer thickness was fixed to 3 cm for a particle radius of 2.5 mm. Figure 2 shows a sample slice of a generated weak layer.

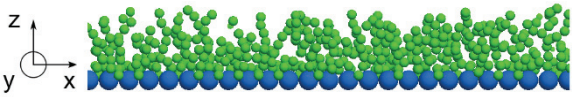

Figure 2: System coordinate and slice of the generated weak layer.

The simulation of mixed-mode shear-compression experiments allowed evaluating the failure envelope, which was in good qualitative agreement with experimental data (Reiweger and Schweizer 2013). Variations in particle deposition did not influence the failure envelope. Unconfined load-controlled compression tests with fixed bond

strength and varying elastic modulus of the particles revealed a linear relation with the macroscopic elastic modulus. In addition, by fixing the particle elastic modulus and varying the bond strength, a linear relation with the macroscopic weak layer strength was obtained. These results allowed defining the macroscopic behavior of the weak layer as a function of particle and bond parameters.

2.5 PST generation

Based on the slab and weak layer generation and characterization, we generated a 2 m long and 30 cm wide PST beam composed of a completely rigid basal layer, a weak layer of thickness D_{wl} = 3 cm and a slab of thickness D_{slab} = 45 cm. We assumed a weak layer macroscopic elastic modulus of 1 MPa and the slab macroscopic elastic modulus of 6.5 MPa (van Herwijnen, Gaume et al. 2016). The weak layer compressive strength was assumed to be σ_c^{wl} = 3.2 kPa, which corresponds to a critical crack length a_{c} = 33 cm for the onset of crack propagation. The slab compression strength σ_c^{slab} was varied (see results). The snow saw was modeled as a rigid wall which moves into the weak layer with constant speed v_{saw} = 1 m/s. As soon at weak layer bonds broke further than 20 cm ahead of the saw tip, the saw was removed. The weak layer normal stress σ_{z} was computed as the mean stress at the interface between the weak layer and the substratum every 2 cm, in the x direction.

3. RESULTS

3.1 Unconfined compression of the weak layer

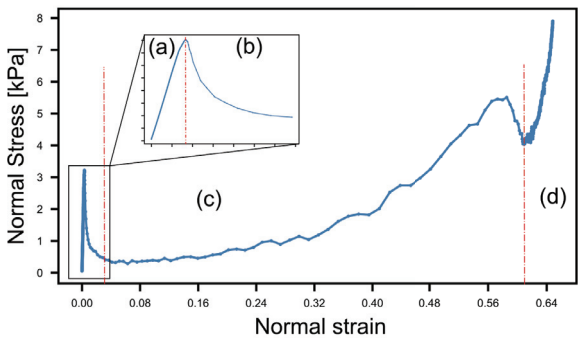

Figure 3: Stress-strain curve for a weak layer sample under unconfined compression: (a) linear elastic phase, (b) softening, (c) collapse, (d) jamming.

The unconfined load-controlled compression tests of the slab and weak layer configuration showed a linear relation between the elastic modulus of the particles and the macroscopic elastic modulus (Figure 1). It also illustrated the generic material behavior consistent with laboratory experiments (e.g., Capelli, Reiweger et al. 2018). Figure 3 shows an example of the evolution of the average normal stress $\overline{\sigma_z}$ measured at the interface between the rigid base and the weak layer as function of the normal strain ε_{z}. The normal strain is computed as $\epsilon_{\mathrm{z}} = u_{\mathrm{z}}/D_{\mathrm{wl}}$ where u_{z} is the displacement of the compressive wall. The macroscopic weak layer parameters were the same as the PST parameters described above. During this simulation, four stages can be distinguished. First, a linear elastic behavior without critical bond breaking (a). When the macroscopic strength is reached, the normal stress significantly drops and a softening phase starts (b). After the softening phase, the sample repeatedly collapses (crushing phase) during which ε_{z} substantially increases (c). Finally, after the repeated collapses, the jamming phase starts where density and stress increase (d).

3.2 PST: Comparison with field data

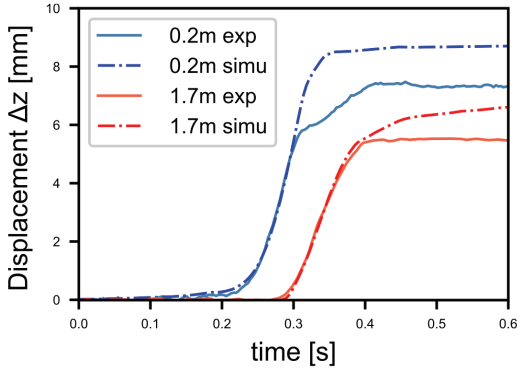

Figure 4: Slab displacement during a PST. The blue color corresponds to the saw-side of the PST (0.2 m from the edge) and the red color to the end of the beam (1.7 m from the edge). Solid lines refer to the experiment, dashed lines to the simulation.

We compared our PST simulation to a field experiment that had similar geometry and mechanical properties as our model (Figure 4). Based on the particle tracking analysis of the video images taken during the experiment, the normal displacement Δz was computed as function of time (solid lines in Figure 4). For the DEM simulation, the temporal evolution of the slab displacement Δz exhibited very similar behavior (dashed lines in Figure 4). Two distinct phases are obvious: bending of the slab when the vertical displacement slowly increases at the sawing side (up to 0.21 s) followed by crack propagation and weak layer fracture when slab displacement rapidly increases, even at the right-end of the beam with a delay of ~0.1 s. At 0.37 s, the slab touches the bed surface, which consists of fragmented weak

layer crystals and the base; the largest displacement is observed at the saw-side of the beam in both the field experiment and the DEM simulation. After 0.4 s the weak layer is completely fractured and the entire slab touches the bed surface. At the end of the process, simulation and experiment do not perfectly match. This discrepancy is likely due to a differences in weak layer porosity and thickness.

3.3 PST: Crack propagation analysis

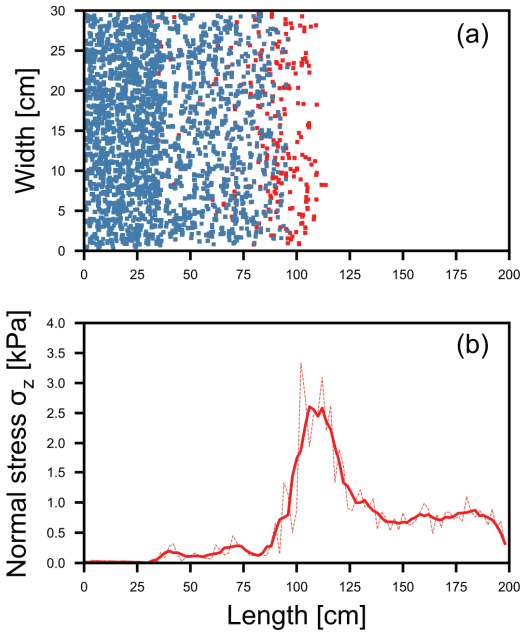

Figure 5: (a) Top view of the weak layer bond states: in blue broken bonds, in red bonds breaking at current time step. (b) Normal stress σ_z along the length of the PST at the corresponding time step during the dynamic crack propagation process.

As in DEM simulations we have access to every particle state, the dynamics of crack propagation can be analyzed from bond breaking and the stress distribution. Figure 5 shows the results of the particles states at a given time step during the crack propagation process. In the upper plot a top view of the weak layer bond states is shown. The position of already broken bonds is shown in blue, while currently breaking bonds are shown in red. Between 0 and 33 cm there are more broken bonds than beyond 33 cm, which corresponds to the part of the beam where the bonds were broken by the saw. Broken bonds can be seen up to a distance of 1 m, which correspond to the position of the crack tip. The normal stress σ_z along the length of the PST is measured at the interface between base and weak layer (Figure 5b). From 0 to about 35 cm there is no stress as due to the saw cut the weak layer is destroyed and at this time step the slab is not yet in contact with the bed surface. The stress between 35 and 80 cm corresponds to the residual stress induced by the weight of the fractured weak layer. From 80 to 110 cm the stress increases, corresponding to the fracture process zone where the material undergoes strain-softening. Between 110 and 150 cm the normal stress is highly concentrated; this stress concentration will drive the crack propagation at the next time step. From 150 cm to the end of the beam the normal stress corresponds to the static load induced by the weight of the slab and the weak layer due to gravity. The reduction of the normal stress at the very end can be attributed to edge effects in the simulation.

3.4 Preliminary results for a PST on a slope

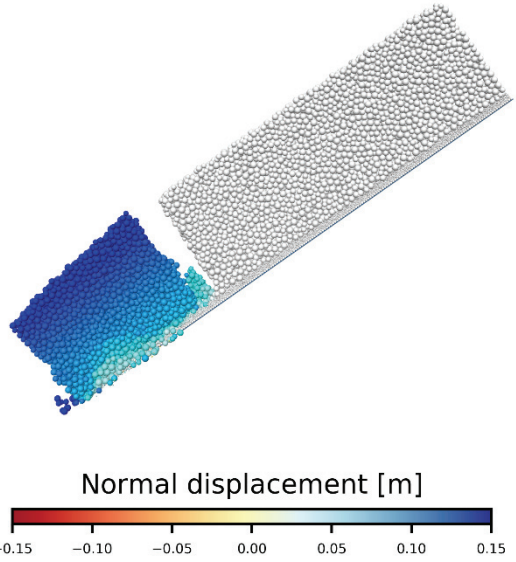

Figure 6: PST state on a slope after two seconds of simulation from the beginning of the sawing. The colors correspond to the displacement normal to the slope.

We also simulated a PST on a slope with an angle of ψ = 35°. The slab macroscopic compressive strength was set to σ_c^{slab} = 5.4 kPa to allow for slab fracture. Figure 6 shows the PST state after 2 s of simulation. The plot is colored according to the slope normal displacement. The critical crack length in this simulation was a_c = 22 cm and a slab fracture appears from the top of the slab at 55 cm from the lower edge of the beam. This simulation is in agreement with slab fracture behavior observed in field experiments: short crack propagation followed by a slab fracture from the top and subsequent sliding of the slab.

4. DISCUSSION AND CONCLUSIONS

We presented a 3D-model of a PST experiment using the discrete element method with elastic-brittle bonded particles. The model allows studying weak layer failure and crack propagation in quasi-brittle layered media such as snow.

By tuning the parameters characterizing the particles and bonds we can tune the DEM to reproduce a large range of observed macroscopic mechanical snow properties. Highly porous weak layers were obtained with a 3D cohesive ballistic deposition technique. Standard ballistic deposition was used to generate a dense snow slab. We found a linear relation between macroscopic properties such as the elastic modulus and the compressive strength with the corresponding microstructural parameters of particles and bonds. Hence the model reproduced macroscopic mechanical snow behavior without the need to take into account the full complexity of snow microstructure.

By performing simulations of a PST, we were able to reproduce quasi-static slab bending, dynamic crack propagation, weak layer collapse as well as slab fracture. Simulation results were in good agreement with field experiments. In addition, the DEM method provides insight into the mechanical properties and the stress distribution during the fracture process. However, these findings cannot be validated as long as no theoretical framework or stress measurements during field experiments are available.

In the future, we plan to relate snowpack properties to crack propagation speed and the stress distribution. Eventually we plan to extend the model to the scale of an avalanche slope.

REFERENCES

Capelli, A., et al. (2018). "Acoustic emissions signatures prior to snow failure." Journal of Glaciology **64**: accepted for publication.

Cundall, P. A. and O. D. L. Strack (1979). "A discrete numerical model for granular assemblies." Géotechnique **29**(1): 47-65.

Gaume, J., et al. (2017). "Scaling laws for the mechanics of loose and cohesive granular materials based on Baxter's sticky hard spheres." Physical Review E **96**(3): 032914.

Gaume, J., et al. (2015). "Modeling of crack propagation in weak snowpack layers using the discrete element method." The Cryosphere **9**: 1915-1932.

Gauthier, D. and J. B. Jamieson (2006). "Towards a field test for fracture propagation propensity in weak snowpack layers." Journal of Glaciology **52**(176): 164-168.

Hagenmuller, P., et al. (2015). "Microstructure-based modeling of snow mechanics: a discrete element approach." The Cryosphere **9**(5): 1969-1982.

Kadau, D. and H. J. Herrmann (2011). "Density profiles of loose and collapsed cohesive granular structures generated by ballistic deposition." Physical Review E **83**(3): 031301.

Löwe, H., et al. (2007). "On the evolution of the snow surface during snowfall." Geophysical Research Letters **34**(21).

McClung, D. M. (1979). "Shear fracture precipitated by strain softening as a mechanism of dry slab avalanche release." Journal of Geophysical Research **84**(87): 3519-3526.

Potyondy, D. O. and P. A. Cundall (2004). "A bonded-particle model for rock." International Journal of Rock Mechanics and Mining Sciences **41**(8): 1329-1364.

Reiweger, I. and J. Schweizer (2013). "Weak layer fracture: facets and depth hoar." The Cryosphere **7**(5): 1447-1453.

Schweizer, J., et al. (2003). "Snow avalanche formation." Reviews of Geophysics **41**(4): 1016.

Sigrist, C. and J. Schweizer (2007). "Critical energy release rates of weak snowpack layers determined in field experiments." Geophysical Research Letters **34**(3): L03502.

van Herwijnen, A., et al. (2016). Measuring the mechanical properties of snow relevant for dry-snow slab avalanche release using particle tracking velocimetry. Proceedings ISSW 2016. International Snow Science Workshop, Breckenridge CO, U.S.A., 3-7 October 2016.

van Herwijnen, A., et al. (2016). "Estimating the effective elastic modulus and specific fracture energy of snowpack layers from field experiments." Journal of Glaciology **62**(236): 997-1007.

van Herwijnen, A. and B. Jamieson (2005). "High-speed photography of fractures in weak snowpack layers." Cold Regions Science and Technology **43**(1-2): 71-82.

van Herwijnen, A., Gaume, J., Bair, E.H., Reuter, B., Birkeland, K.W. and Schweizer, J., 2016. Estimating the effective elastic modulus and specific fracture energy of snowpack layers from field experiments. J. Glaciol., 62(236), 997-1007.